Computer Modeling in Engineering & Sciences
DOI:10.32604/cmes.2020.09923
Article

Tech Science Press

Numerical Simulation of Multi-Layer Penetration Process of Binder Droplet in 3DP Technique

Xiangyu Gao, Weidong Yang*, Hongxuan Xian, Xiyuan Tu and Yuanyuang Wang*

School of Mechanical Engineering, Hebei University of Technology, Tianjin, 300130, China
*Corresponding Authors: Weidong Yang. Email: yangweidong@hebut.edu.cn; Yuanyuan Wang. Email: 2012047@hebut.edu.cn
Received: 28 January 2020; Accepted: 19 March 2020

Abstract: This paper studies the binder droplet injection process in the 3DP technique. The mathematical model of the binder penetration process for multi-nozzle and multi-layer in 3DP technique is established, by using the conservation Level set method. According to the two-dimensional plane model of three-dimensional spatial structure of sand bed, the construction method of an equivalent cylindrical mapping infiltration model is proposed to represent the porosity of the model in the two-dimensional plane, which is exactly the same as that in the three-dimensional space, as well as closer to the arrangement of the three-dimensional space, and to realize the differentiation between the pores and the throats. The method of spraying droplets alternately by multiple nozzles simulates the staggered arrangement of multiple array-type nozzles and prints the current layer completely at one time. The numerical simulation of multi-layer penetration process is realized by using the method of continuous multi-simulation. The simulation model of the binder penetration process by using multi-nozzle and multi-layer is established to simulate the whole process of the binder from the nozzle to impacting on the sand bed and then to penetrating into the sand bed, which reflects the complete penetration process and predicts the sand agglomeration.

Keywords: Additive manufacturing; binder penetration; numerical simulation; level set method; three-dimensional printing

1 Introduction

Three-dimensional printing (3DP) technique refers to a group of emerging technologies for fabricating physical objects directly from computer-based geometrical descriptions of part designs [1]. The technique starts with the spreading of a thin layer of powder material on a building platform to form a paper-thin medium, followed by bonding the powder selectively through printing of a binder liquid through the inkjet nozzle at the area defined by the graphical data in the computer [2].

3DP technique has the advantages of shortened manufacturing time, reduced costs, and unlimited model complexity. It has become one of the most popular manufacturing technologies nowadays [3].

In the paper, 3DP process is utilized in spraying the binder to the surface of the laid sand bed through the nozzle. The technique is characterized by the injection molding of the binder and the subsequent interaction with the sand bed. The collision and penetration of the binder and the sand bedding is the key to the accuracy of the 3DP process.

The spread and penetration behaviors of the droplets in porous material are specified by the extension diameter, the penetration depth, and the penetration time, which are affected by the process parameters including the impact velocity of the droplet, the viscosity of the binder liquid, the features of the powder bed, the wettability of the liquid in the porous medium, and the mutual influence of multi-droplet impacting on the bed at the same time.

Previous studies were mostly focused on the study of the dynamics of droplet impacting on the surface of porous media. In these studies [4,5], a high-speed camera was used to record the change of droplets on the surface of the powder layer. However, the permeation process of droplets in the powder bed could not be observed with the instruments directly. The process of droplet impinging on powder bed is complicated and has been mainly observed and analyzed by the experimental studies. However, these were often restricted by the experimental conditions, with the pressure field and velocity field of the droplets inside the bed being difficult or impossible to measure.

Tan [6] proposed to use the direct numerical simulation to study the micron-sized droplets impacting on the powder bed, and conducted two numerical tests. Kim et al. [7] applied the volume of fluid (VOF) method to calculate the impact of droplets on the porous media. In the VOF advection equation, the compression term was added to estimate the VOF function accurately.

Gao et al. [8] presented a combined finite element/discontinuous Galerkin/level set method to simulate the incompressible two-phase flow. The level set method was employed to capture the moving interface because of its simplicity and efficiency when dealing with the significant interface deformations.

Moataz et al. [9] described a new numerical scheme to model the surface tension in the two-phase flow, with the interface represented by a level-set function. Application to the Marangoni breakup of an axisymmetric droplet showed that the method was robust also in the case of changing in the interface topology.

Konstantinos et al. [10] presented a coupling method of the level set and VOF methods, based on a simple local-gradient based re-initialization approach that evaluates the distance function depending on the computational cell location. This coupled method had better accuracy than the VOF method alone, and was capable of capturing sharp interfaces in all the classical numerical tests.

Karim [11] developed a robust numerical scheme to predict the equilibrium interfaces over arbitrary solid surfaces. This framework avoided the reinitialization that is typically used in traditional level set methods.

Chakrabort [12] studied some fundamental aspects of rising gas bubbles in stagnant Newtonian liquids using a coupled level-set and VOF method. The coupled method not only represented the geometric properties (normal and curvature) of the bubble surface accurately but also satisfied the compliance of mass conservation very well.

Chen [13] provided sensitivity analysis for the formulated compliance- and stress-minimization problems, where a novel strategy called the adaptive level set adjustment was proposed to remedy the deficiency of ignoring the non-implementable sensitivity terms.

Bellotti [14] presented a novel hybrid method combining the reference map theory with the level-set method for tracking the moving interfaces. The coupled method was extensively validated in the case of externally generated velocity fields and incorporated into the previously introduced two-phase incompressible Navier-Stokes flow solver.

Bahbah [15] presented a high fidelity conservative and adaptive level-set method for the simulation of two-fluid flows. Anisotropic meshing with conservative interpolation was implemented and tested on several benchmarks including splashes, sloshing and complex bubble dynamics.

Cui et al. [16] studied the effect of pore distribution on solid-liquid properties. The liquid-liquid interface in the disordered porous media was tracked by the VOF method. In order to study the process of droplet infiltration more intuitively, Wang et al. [17] established the infiltration model, analyzed the effects of the contact angle, the porosity, and the drop height on the infiltration by using COMSOL software in the simulation.

Amiri et al. [18,19] proposed the level set model of two-phase flow permeation of the heterogeneous porous media and simplified heterogeneous porous media, and compared the CFD analysis results with that using the actual complex porous media model. The calculation time for using the simplified porous media model was reduced greatly, while the permeability trend was maintained, which proved that the pore media model using the regular spheres instead of the actual porous media causes negligible influence to the CFD prediction results.

2 Mathematical Model of Porous Media Permeation Process

This study uses the level set method to tract the moving boundary. The Level Set method was first proposed by Osher [20] for the calculation of two-phase flow in 1988. It is a method to calculate and analyze the interface motion in two-dimensional or three-dimensional space. The Level set method can capture the interface accurately. No matter how the flow field changes, the distance function keeps smooth, and it can well deal with the complex interface deformation and the topology change. The method has conservation property and there is no loss of physical quantity in the calculation process. The application of this method can better deal with complex motion interface problems.

2.1 Phase Interface Tracking Equation

In order to track the droplet morphology after dropping, the Level set method is used to describe the two-phase interface. Let ϕ represent the isohypse line of the Level set function in the fluid interface, with $\phi = 0$ for the air, and $\phi = 1$ for the binder. ϕ transitions from 0 to 1 smoothly, and the interface moves with the fluid velocity u on the interface. Therefore, the horizontal set function can be regarded as the volume fraction of the fluid. The function of the fluid interface separating the two phases is expressed as

$$\frac{\partial \phi}{\partial t} + \nabla \cdot (\boldsymbol{u}\phi) = \gamma \nabla \cdot \left(\varepsilon \nabla \phi - (1 - \phi) \frac{\nabla \phi}{|\nabla \phi|} \right) \tag{1}$$

where u is the velocity of the fluid, γ is the reinitialization parameter in the solution of the equation. ε is the interface thickness, whose value can be set as half of the grid generation unit in the calculation model. t is the two-phase time.

Due to the inherent influence of the level set function, the properties of the distance function are unlikely to be well preserved over several time steps. Therefore, the Level set needs to be reinitialized after each step. Eq. (2) describes the convection of the reinitialized level set function [21].

$$\frac{\partial \phi}{\partial t} + \nabla \cdot (\phi \boldsymbol{u}) + \gamma \left[\left(\nabla \cdot \left(\phi(1 - \phi) \frac{\nabla \phi}{|\nabla \phi|} \right) \right) - \varepsilon \nabla \cdot \nabla \phi \right] = 0 \tag{2}$$

2.2 Transport Characteristics of Mass and Momentum

When the velocity Mach number of the fluid and air is less than 0.3, the density change in the flow process can be completely ignored and the flow can be regarded as incompressible flow. The governing equations describing this fluid are mainly the incompressible Navier-Stokes equations. In the process of droplet injection, the velocity of droplet and air is much lower than that of the sound, which can be regarded as incompressible flow.

Navier-Stokes equations include the surface tension, a motion equation describing the conservation of momentum in a viscous incompressible fluid. Navier-Stokes equations are:

$$\rho\left(\frac{\partial u}{\partial t}+\boldsymbol{u}\cdot\nabla\boldsymbol{u}\right)-\nabla\cdot\left(\mu\left(\nabla\boldsymbol{u}+\nabla\boldsymbol{u}^{\boldsymbol{T}}\right)\right)+\nabla P=F_{st} \quad (3)$$

$$(\nabla\cdot\boldsymbol{u})=0 \quad (4)$$

where ρ is the density (kg/m^3), μ is the dynamic viscosity (N·s/m^2), $\boldsymbol{u}$ is the velocity (m/s), P is the pressure (Pa), and F_{st} is the surface tension.

After smooth treatment, the density and viscosity of the fluid can be expressed as Eqs. (5) and (6).

$$\rho=\rho_{air}+(\rho_{water}-\rho_{air})\phi \quad (5)$$

$$\mu=\mu_{air}+(\mu_{water}-\mu_{air})\phi \quad (6)$$

The surface tension is calculated by Eqs. (7) and (8).

$$F_{st}=\nabla\cdot T \quad (7)$$

$$T=\sigma\left(I-\left(nn^{T}\right)\right)\delta \quad (8)$$

I is the identity matrix, n is the entry normal vector. σ is the surface tension coefficient (n/m), and δ is equal to a non-zero Dirac delta function.

The normal vector of the inlet is express as

$$n=\frac{\nabla\phi}{|\nabla\phi|} \quad (9)$$

The delta function is approximated by Eq. (10).

$$\delta=\ 6|\phi(1-\phi)| \quad (10)$$

3 Construction of the Simulation Model

3.1 Sand Bedding Modeling-Equivalent Cylinder Method

In this paper, an osmotic model is built for the sand in the sand molds. The sand bedding is a three-dimensional space, while for simplification this study is a two-dimensional analysis, and using a two-dimensional plane to simulate the sand bedding. For this reason, the parameters of the two-dimensional description need to be properly adjusted, to achieve a mapping from the three-dimensional space to the two-dimensional space to ensure the accuracy of the simulation results.

For the particles in the sand bed, the main factors influencing the permeability are their spatial configuration law (pore and shouted distribution) and the porosity. The droplets in the process of permeability mainly flow in the holes in the sand bedding, the configuration of the sand space determines the final shape of the liquid penetration, and the size of the pores determines the results of their penetration. The porosity is closely related to the space configuration, which is not easy to change by adjusting the distance between the sand particles, so the transformation of the sand bedding from three-dimensional space to two-dimensional space need to make sure that the space configuration rule matches the porosity.

The particles arrangement in two-dimensional cross section for different sand bedding are shown in Fig. 1. The arrangement of the two-dimensional space only takes into account the particles at a certain section of the configuration, while does not consider the spatial arrangement of the particles. Since the different cross sections are arranged in the different way, this configuration cannot reflect the arrangement of actual sand well. Using a single cross-section arrangement can cause mismatch of porosity between the 3D and 2D situations.

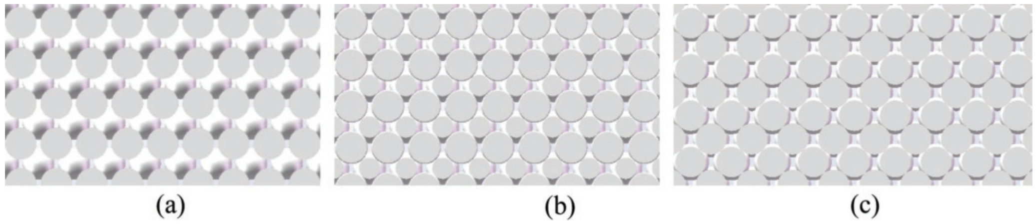

Figure 1: Distribution of sand particles in different sections. (a) Sand bedding section, (b) The section in "(a)" is moved back 20 μm and (c) The section in "(a)" is moved back 40 μm

Since the two-dimensional plane is unable to reflect the spatial configuration of the sand particles, this study proposes to use the equivalent cylindrical elements to replace the spherical particles. In a certain space, using along a certain direction parallel to the original sand concentric cylinder instead of the original sand, the use of parallel cylindrical replaces the guarantee sand bed porosity, arbitrary in vertical direction of the cylindrical section between particles that can be exactly the same configuration, so the cylindrical section can be used for the simulation calculation of two-dimensional plane.

The direction of the arbitrary symmetry axis is selected as the direction of the equivalent cylinder to establish the penetration model of the equivalent cylinder, as shown in Fig. 2.

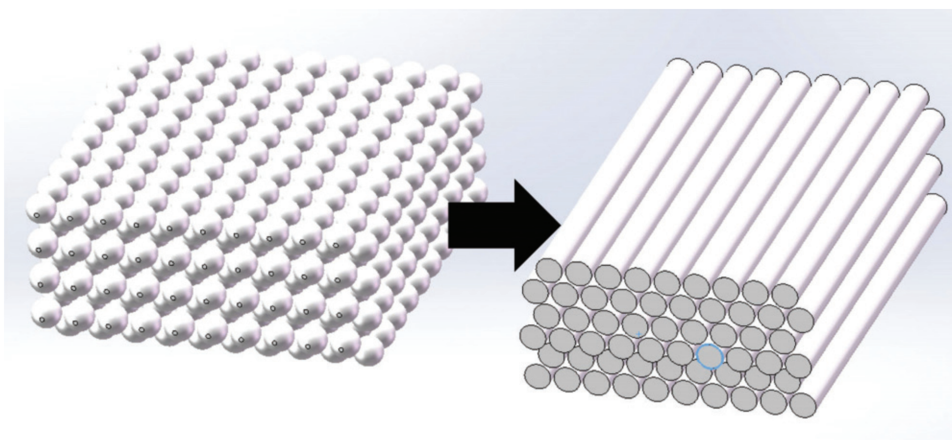

Figure 2: Substitution schematic of the equivalent cylinder (arrangement not calculated)

According to the CT scan of the sand samples, the porosity of the sand bed is 0.376, and the arrangement of sand particles is close to the arrangement of the orthocline cube. The model is established by using the arrangement parameters of the orthocline cube (in vertical direction), as shown in Fig. 3a. The particles are arranged in an isosceles triangle with a spacing of $2r$ and an included angle of 60°. The direction perpendicular to the paper is chosen as the direction of the cylinder. The positions of the center of the circle of the original particles remain unchanged. The cylinder is used to construct the equivalent cylinder model instead of the original spherical particles (as shown in Fig. 3b).

The volumes before and after conversion are the same.

Sphere volume is expressed as

$$V = \frac{4}{3}\pi r^3 \tag{11}$$

Cylinder volume is expressed as

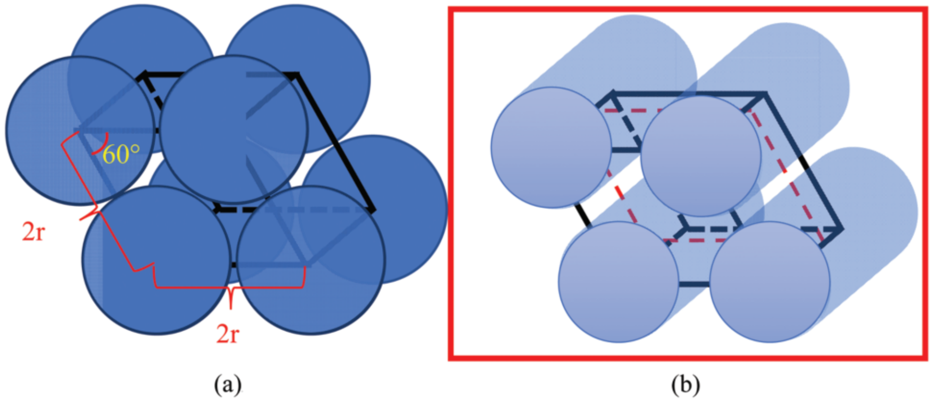

Figure 3: Construct the equivalent cylinder model. (a) Arrangement of positive rhombic bodies and (b) Arrangement of positive rhombic bodies equivalent cylinders

$$V = \pi r_0^2 d \tag{12}$$

where V is the volume, r is the radius of the sphere, r_0 is the equivalent radius of the cylinder, and d is the distance between the center of the two spheres. The radius of the cylinder is expressed as

$$r_0 = \sqrt{\frac{4r^3}{3d}} \tag{13}$$

This study uses the COMSOL 5.3a software for the analysis, for this a two-dimensional simulation model of the sand bed is established, as shown in Fig. 4. The circular particles are sand particles with an equivalent radius of 65.7 μm, and the porosity of the material is 0.3954. The resolution of the narrowest area of the sand bed is 3 grid.

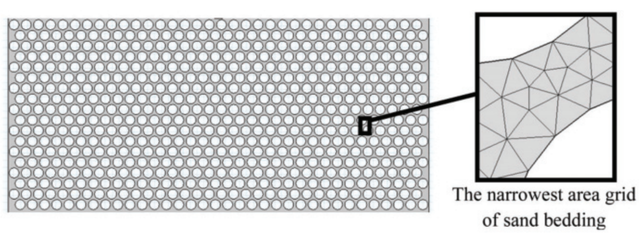

Figure 4: Part model of COMSOL sand bedding

3.2 Construction of the Array Nozzle Model

In the existing 3DP technique, multiple array-type nozzles are staggered to print the whole layer at one time.

According to the nozzle parameters of the manufacturer, a simulation model is built. Each nozzle contained 256 sprinkler heads, which are designed as inverted trapezoid, with a diameter of 54 μm at the top and 50 μm at the bottom. The spacing D between the heads is 256 μm. In this paper, a 2 mm area is to build the simulation model of a nozzle. Each nozzle has 6 sprinkler heads, as shown in Fig. 5.

Pressure signal *PP0* with a periodically varying amplitude of 47 kPa is applied at the head inlet, which is expressed as

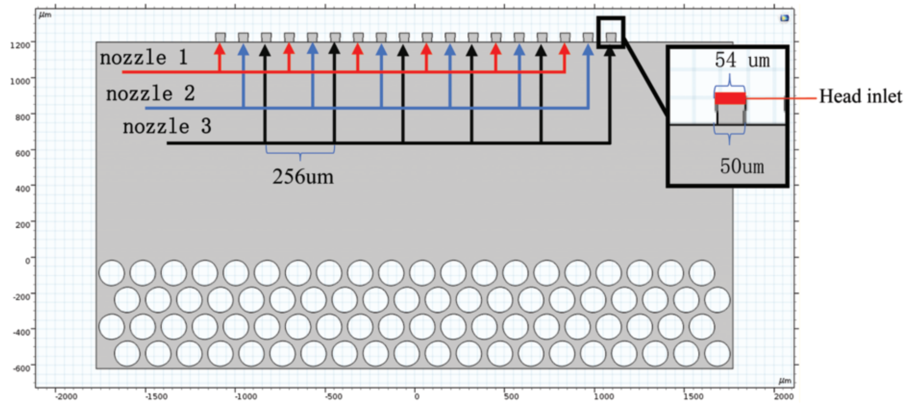

Figure 5: Geometric diagram of the simulation model of three nozzles

$$PP0 = 47[kPa] * pw1(t[1/s]) \tag{14}$$

where, *pw1*(*t*[*1/s*]) is the pressure pulse signal, as represented by Eq. (15):

$$pw1(t[1/s]) = \begin{cases} 1, & 0 + n \times T < t < 2 \times 10^{-6} + n \times T \\ -1, & 2 \times 10^{-6} + n \times T < t < 40 \times 10^{-6} + n \times T \\ 0, & \text{others} \end{cases} \tag{15}$$

where n represents the number of layers, T represents the period of the injection cycle, which is 3 ms, and t represents the time. Firstly, a positive pressure of 2 µs duration is applied on the head to eject the droplets, then a negative pressure of 38 µs duration is applied to break the droplets away from the head. Then, the pressure is maintained at 0 Pa.

3.3 Construction of the Multi-Layer Infiltration Model

The initial and boundary conditions are shown in Tab. 1. In the COMSOL software, the head inlet cannot be moved during the simulation process, so the space of multi-layer sand particles below the nozzle is reserved in advance. In Fig. 6, ϕ = 0 corresponds to the binder material (the blue part), ϕ = 1 for the air (the red part), and ϕ = 0.5 for the two-phase interface (the green part). The white cycles are the sand particles.

Table 1: Initial and boundary conditions

Project	Parameters
Inlet	Boundary Condition: Pressure *PP0*
Outlet	Boundary Condition: Pressure 0 Pa
Wetting wall	Wetted wall: Contact angle pi/6; Slip length 5 µm
Initial interface	Initial Values: Velocity field 0 m/s; Pressure 0 Pa

This study deals with the multi-layer fabrication process. For this a separate domain model is created for the calculation when each of the new layer is added. During the calculation, when the analysis on the current layer domain model is finished, the flow variables are interpolated onto the next domain model corresponding to one with the new layer added, and the CFD computation is then conducted on the refreshed domain model. This way the calculation is repeated until finished with the final domain with all the layers included.

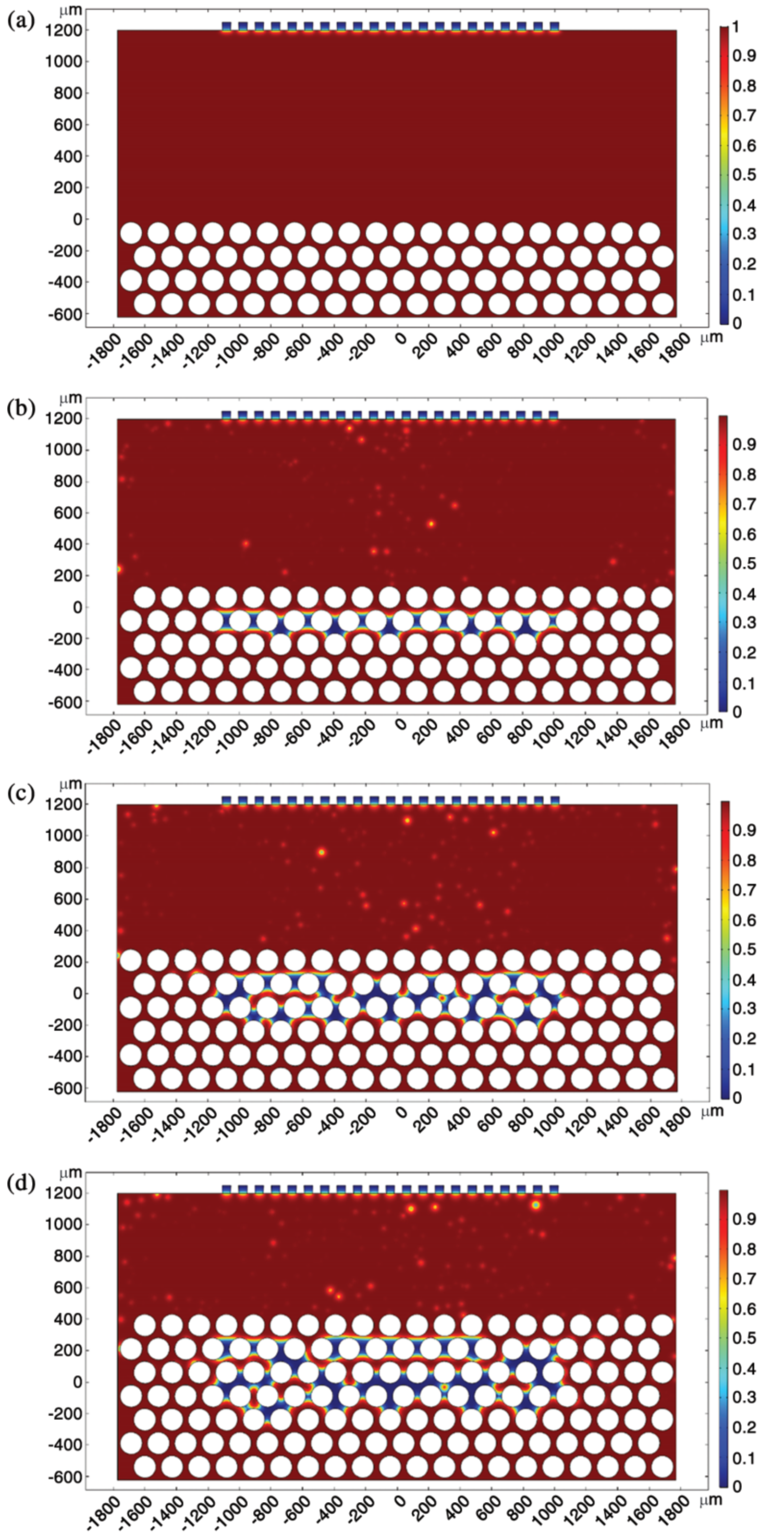

Figure 6: (Continued)

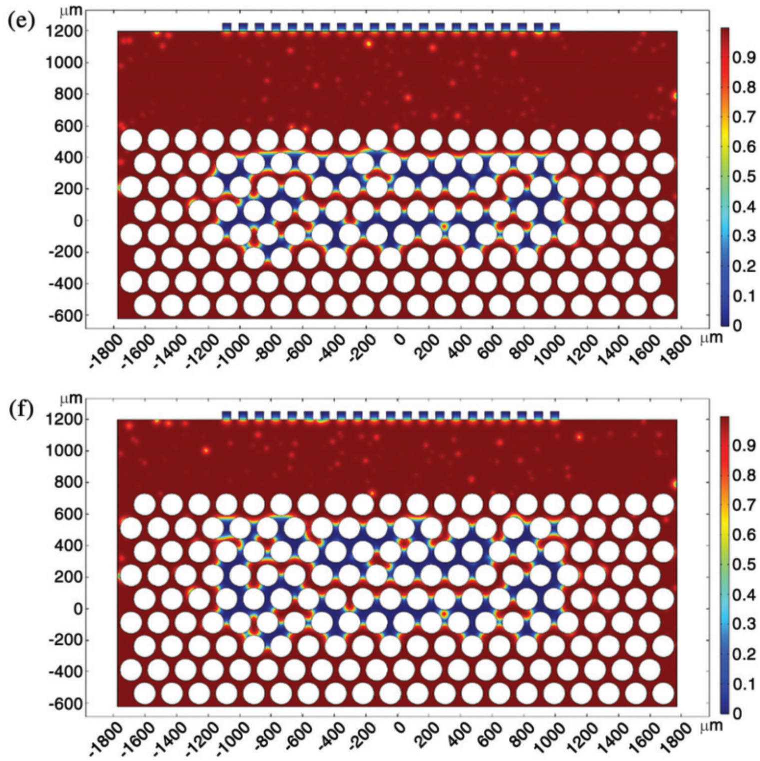

Figure 6: Construction of multi-layer infiltration model. (a) First layer initial state (b) After the first layer infiltration, the sand particles are laid on the second layer (c) After the second layer infiltration, the sand particles are laid on the third layer (d) After the third infiltration, the sand particles are laid on the fourth layer (e) After the fourth layer infiltration, the sand particles are laid on the fifth layer and (f) After the fifth layer infiltration, the sand particles are laid on the sixth layer

4 Simulation Results

The different penetration states of droplets between sand particles are shown in Fig. 7. These include swing, chain, capillary and immersion [22].

The simulation of three nozzles is taken as an example during droplet spraying process. The heads of the same nozzle spray the binder at the same time, whose physical parameters are shown in Tab. 2 [17]. The three nozzles spray the droplet in sequence with the time interval of 400 μs.

Six layer-thick condensation units are obtained after six droplet injection steps are finished, as shown in Fig. 8.

As shown in Fig. 9, the proportion of the binder on line segments A_1 and A_2 is defined as the bonding rate of the two adjacent layers of the infiltration process. This represents the binder ratio between the current layer and the previous layer, with the value in the range of 0%~100%. The closer the measured value is to 100%, the better the bonding effect between the upper and lower layers. The proportion of the binder within the rectangle BCDE represents the content binder in a chosen layer, with the value in the range of 0%~45% (evaluated by measuring the rectangle BCDE after removing the sand area in the largest can accommodate the binder area), represents the different forms of infiltration between the sand particles. The closer the measured value is to 45%, the better the bonding effect between the layers. When the measured value is equal to 45%, the state of droplets between sand particles is in the immersion state, as represented by Fig. 7d.

The number of nozzles is set as 2, 3 and 4 for numerical simulation respectively. When the nozzle number is 2, the volume of the droplet is less. The binder content of each layer is about 12.27% on average, bonding the

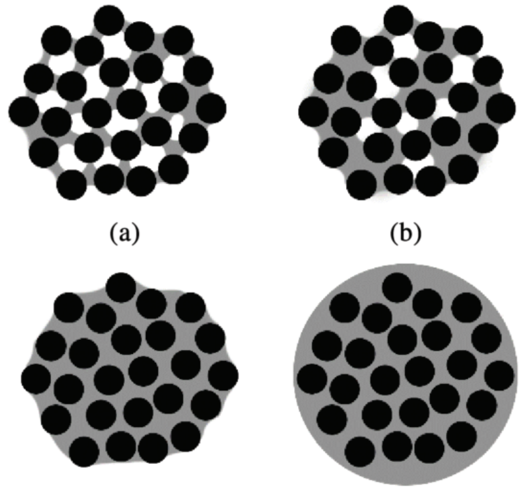

Figure 7: Permeability morphology between sand grain. (a) Swing state (b) chain state (c) capillary state and (d) immersion state

Table 2: Physical parameters of binder

Parameter	Value
Surface tension	3.42×10^{-3} N/m
Dynamic viscosity	9.757×10 mPa*s
Contact Angle	32°
Density	1.120×10^{3} kg/m^{3}

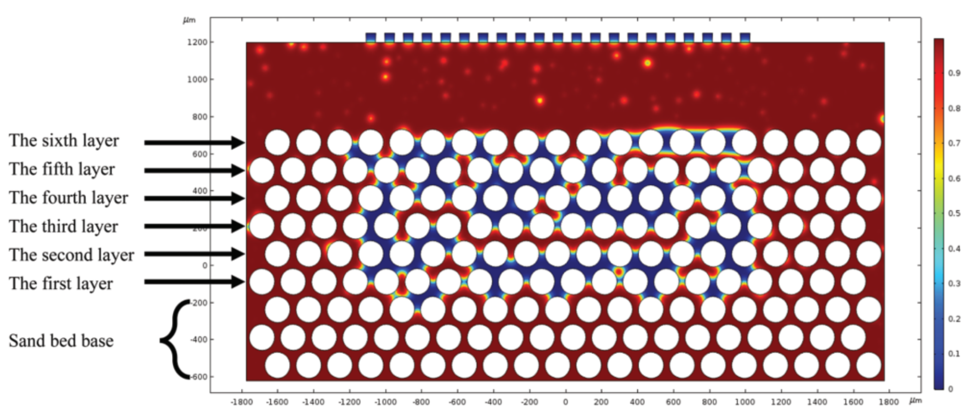

Figure 8: Condensation unit body

sand particles of the same layer effectively. The droplets in the same layer exists swing state. The bonding rate of the two adjacent layers is 24.50% on average, not bonding the sand particles between the two layers effectively. The binder content between the first layer and the base layers is almost 0%, which means that no droplets exist between the sand particles of the base layers. The results are shown as Fig. 10.

When the number of nozzles is 3, the binder content is moderate, the average binder content of each layer is about 17.28%, which can effectively adhere to the sand particles of the same layer. The binder

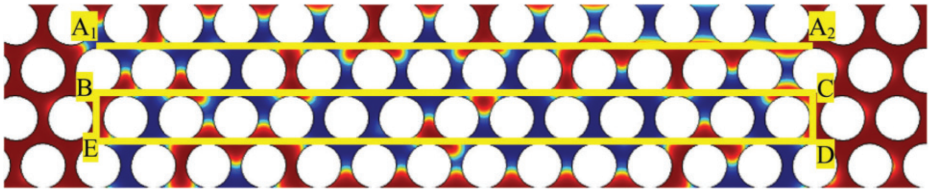

Figure 9: Schematic diagram of measurement area

exists in the chain state between the sand particles, and the bonding rate of the two adjacent layers is 46.94%, which can effectively adhere the upper and lower layers of the sand particles. The bonding rate between the first layer and the neighboring base layers is 27.64%, and the penetration of the first layer has little influence on the sand particles of the next to the base layer. The results are shown in Fig. 11.

When the number of nozzles is 4, the content of the binder is sufficient. The average binder content of each layer is about 21.55%, which can effectively adhere to the sand particles of the same layer. The bonding

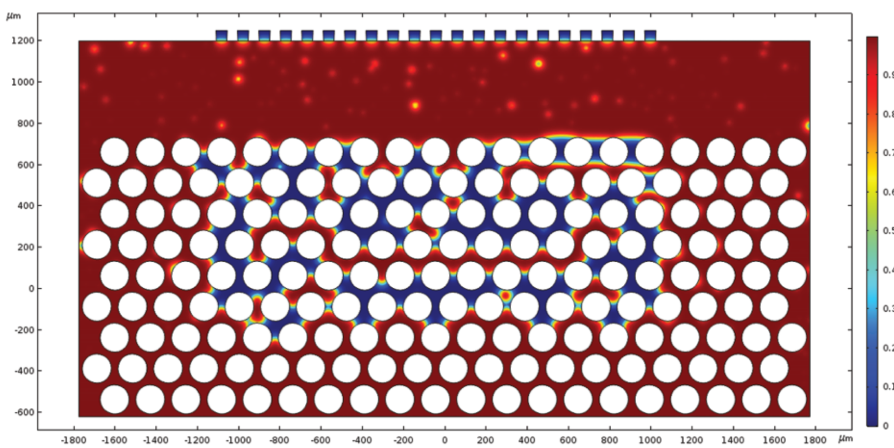

Figure 10: Penetration results of six layers by double nozzles

rate of the two adjacent layers is 57.79%, which can very well adhere to the sand particles of the adjacent two layers. The bonding rate between the first layer and the neighboring base layer is 45.31%, and the penetration of the first layer had a great influence on the sand particles of the neighboring base layer. The another layer beneath the first layer is bonded with the first layer, so the elimination treatment of the corresponding error should be removed, as shown in Fig. 12.

By comparing the simulation results of different number of nozzles, it is observed that as the number of nozzles increases, as shown in Fig. 13. The binder content in the same layer increases, the bonding rate of two adjacent layers increases, and the influence on the sand particles of the base layer also increases, as shown in Fig. 14.

Under the condition of two nozzles, the binder content is low, and the adhesion between the two adjacent layers is poor. When using three nozzles or four nozzles, the bonding rate between the second layer and the third layer, and that between the fifth layer and the sixth layer, are significantly reduced. Fig. 16 shows a normal circumstance where the space of the droplets filling is satisfactory. When excessive binder is applied, the droplets become in contact with the underneath sand bed, which drives away the binder droplets originally penetrated below the current layer (as shown in Fig. 17), and this leads to the decreased binder content in the current layer. This corresponds to the unusual dips in the curves in Fig. 15.

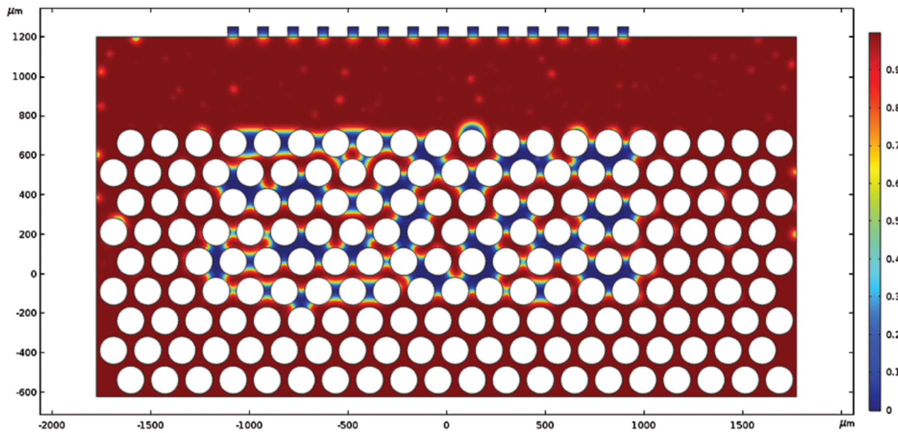

Figure 11: Penetration results of six layers by three nozzles

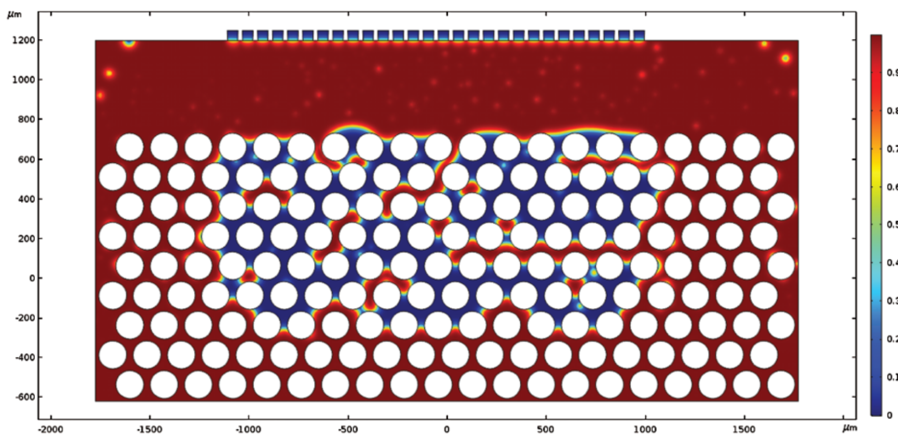

Figure 12: Penetration results of six layers by four nozzles

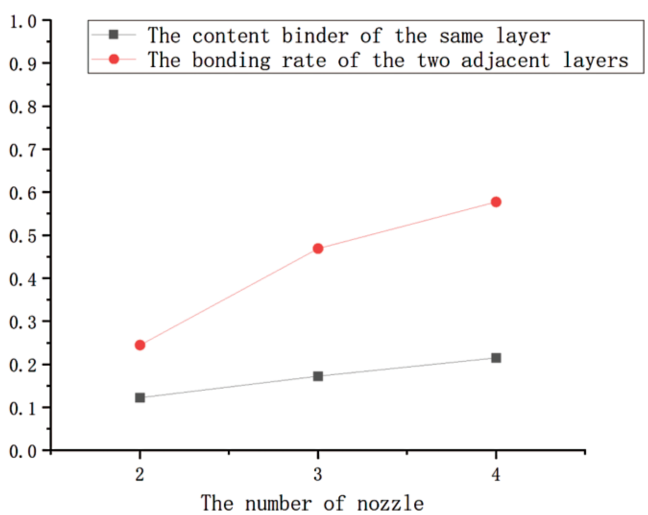

Figure 13: Various trend of the content binder of the same layer and the bonding rate of the two adjacent layers with the number of nozzles

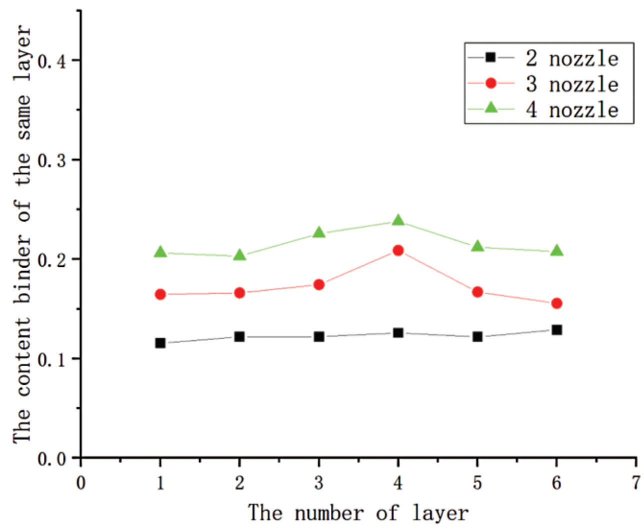

Figure 14: Comparison curves of the content binder of the same layer with different nozzles

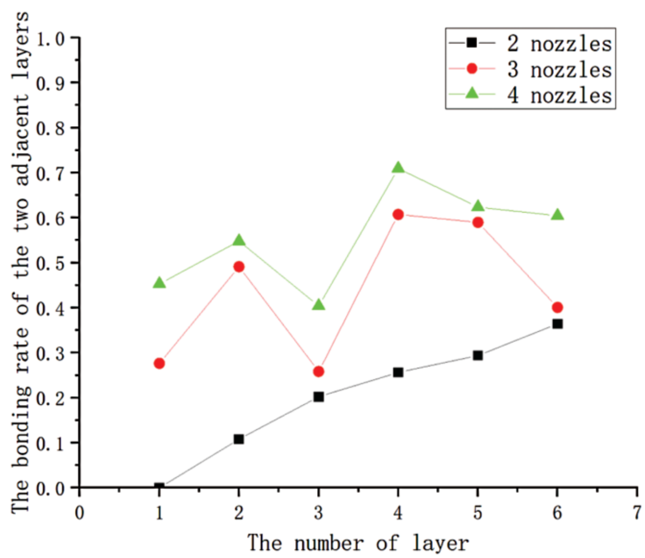

Figure 15: Comparison curves of the bonding rate of the two adjacent layers with different nozzles

Figure 16: Normal droplet filling

Figure 17: Excessive droplet filling

5 Conclusions

1. An equivalent cylindrical penetration model is proposed to simulate the porous structure of the sand bed in 3DP process. The equivalent cylindrical penetration model has the same porosity with the three-dimensional arrangement and is closer to the arrangement of three-dimensional space. The porosity is connected with the spatial structure, avoiding errors caused by only changing the porosity without changing the spatial structure.
2. Simulation models of multiple nozzles are built to simulate the droplet jetting process of the sprinkler heads in 3DP process, and the working state of multi-nozzle spraying process is simulated by changing parameters.
3. The penetration model of multi-layer sand bed is built, which is used for the simulation of multi-layer penetration process in the 3DP process, and for the observation of the flowing process of the binder droplets between the upper and lower layers and the same layer.
4. Numerical experiments are carried out on the simulation model. It is found that when the number of nozzles is constant, the binder proportion of the sand particles in the same layer is relatively stable, which increases with the number of nozzles. In the same condensation unit body, the bonding rate of the two adjacent layers is quite different, indicating that the penetration of each layer is random in a certain range under the same working condition. When the number of nozzles changes, the more the number of nozzles is, the higher the bonding rate of the two adjacent layers is.

The equivalent cylinder penetration model using in the multi-nozzle and multi-layer 3DP application can simulate the binder injection process and the binder infiltration process well. The simulation results are accurate and intuitive, which is helpful for the 3DP development.

Acknowledgement: The authors are thankful for the support from the Natural Science Foundation of Hebei Province, China (Grant No. E2016202297) and the Tianjin science and technology plan project (Grant No. 18YFCZZC00150).

Funding Statement: This research was funded by the Natural Science Foundation of Hebei Province, China (Grant No. E2016202297) and the Tianjin science and technology plan project (Grant No. 18YFCZZC00150). The authors would like to thank for these financial supports.

Conflicts of Interest: The authors declare that they have no conflict of interest to report regarding the present study.

References

1. Diegel, O., Withell, A., Beer, D. D., Potgieter, J., Noble, F. K. (2012). Low-cost 3D printing of controlled porosity ceramic parts. *International Journal of Automation Technology, 6(5),* 618–626. DOI 10.20965/ijat.2012.p0618.
2. Patirupanusara, P., Suwanpreuk, W., Rubkumintara, T., Suwanprateeb, J. (2008). Effect of binder content on the material properties of polymethyl methacrylate fabricated by three dimensional printing technique. *Journal of Materials Processing Technology, 207(1–3),* 40–45. DOI 10.1016/j.jmatprotec.2007.12.058.
3. Butscher, A., Bohner, M., Roth, C., Ernstberger, A., Heuberger, R. et al. (2012). Printability of calcium phosphate powders for three-dimensional printing of tissue engineering scaffolds. *Acta Biomaterialia, 8(1),* 373–385. DOI 10.1016/j.actbio.2011.08.027.
4. Kumar, S. M., Deshpande, A. P. (2006). Dynamics of drop spreading on fibrous porous media. *Colloids and Surfaces A (Physicochemical and Engineering Aspects), 277(1–3),* 157–163.
5. Clarke, A., Blake, T. D., Carruthers, K., Woodward, A. (2002). Spreading and imbibition of liquid droplets on porous surfaces. *Langmuir, 18(8),* 2980–2984. DOI 10.1021/la0117810.
6. Tan, H. (2016). Three-dimensional simulation of micrometer-sized droplet impact and penetration into the powder bed. *Chemical Engineering Science, 153,* 93–107. DOI 10.1016/j.ces.2016.07.015.

7. Kim, W. S., Lee, S. Y. (2016). Behavior of a water drop impinging on porous substrates examination of contact-line drag effect. *Atomization and Sprays, 26(3),* 257–274. DOI 10.1615/AtomizSpr.2015012276.
8. Gao, P. Y., Jie, O., Zhou, W. (2018). Development of a finite element/discontinuous Galerkin/level set approach for the simulation of incompressible two phase flow. *Advances in Engineering Software, 118,* 45–59. DOI 10.1016/j.advengsoft.2018.01.006.
9. Abu-Al-Saud, M. O., Popinet, S., Tchelepi, H. A. (2018). A conservative and well-balanced surface tension model. *Journal of Computational Physics, 371(15),* 896–913. DOI 10.1016/j.jcp.2018.02.022.
10. Lyras, K. G., Hanson, B., Fairweather, M., Heggs, P. J. (2020). A coupled level set and volume of fluid method with a re-initialisation step suitable for unstructured meshes. *Journal of Computational Physics, 407(15),* 109224. DOI 10.1016/j.jcp.2019.109224.
11. Alamé, K., Anantharamu, S., Mahesh, K. (2020). A variational level set methodology without reinitialization for the prediction of equilibrium interfaces over arbitrary solid surfaces. *Journal of Computational Physics, 406,* 109184. DOI 10.1016/j.jcp.2019.109184.
12. Chakraborty, I., Biswas, G., Ghoshdastidar, P. S. (2013). A coupled level-set and volume-of-fluid method for the buoyant rise of gas bubbles in liquids. *International Journal of Heat and Mass Transfer, 58(1–2),* 240–259. DOI 10.1016/j.ijheatmasstransfer.2012.11.027.
13. Qian, C., Liu, J. K., Liang, X., Albert, C. (2020). A level-set based continuous scanning path optimization method for reducing residual stress and deformation in metal additive manufacturing. *Computer Methods in Applied Mechanics and Engineering, 360,* 112719. DOI 10.1016/j.cma.2019.112719.
14. Bellotti, T., Theillard, M. (2019). A coupled level-set and reference map method for interface representation with applications to two-phase flows simulation. *Journal of Computational Physics, 392,* 266–290. DOI 10.1016/j.jcp.2019.05.003.
15. Bahbah, C., Khalloufi, M., Larcher, A. (2019). Conservative and adaptive level-set method for the simulation of two-fluid flows. *Computers & Fluids, 191,* 104223. DOI 10.1016/j.compfluid.2019.06.022.
16. Cui, G. Z., Liu, M. C., Dai, W. J., Gan, Y. X. (2019). Pore-scale modelling of gravity-driven drainage in disordered porous media. *International Journal of Multiphase Flow, 114,* 19–27. DOI 10.1016/j.ijmultiphaseflow.2019.02.001.
17. Wang, Y. Y., Jia, P. F., Yang, W. D. (2018). Simulation and experimental study of binder droplet infiltration in 3DP technology. *Modern Physics Letters B, 32(23),* 1850272. DOI 10.1142/S021798491850272X.
18. Akhlaghi Amiri, H. A., Hamouda, A. A. (2013). Evaluation of level set and phase field methods in modeling two phase flow with viscosity contrast through dual-permeability porous medium. *International Journal of Multiphase Flow, 52,* 22–34. DOI 10.1016/j.ijmultiphaseflow.2012.12.006.
19. Rokhforouz, M. R., Akhlaghi Amiri, H. A. (2019). Effects of grain size and shape distribution on pore-scale numerical simulation of two-phase flow in a heterogeneous porous medium. *Advances in Water Resources, 124,* 84–95. DOI 10.1016/j.advwatres.2018.12.008.
20. Osher, S. (1988). Fronts propagating with curvature-dependent speed: algorithms bose on Hamilton-Jacobi formulations. *Journal of Computational Physics, 79(1),* 12–49. DOI 10.1016/0021-9991(88)90002-2.
21. Olsson, E., Kreiss, G. (2005). A conservative level set method for two phase flow. *Journal of Computational Physics, 210(1),* 225–246. DOI 10.1016/j.jcp.2005.04.007.
22. Zheng, S. L. (2011). *Surface modification of powder*. Beijing: China Building Materials Industry Press.